Lawrence Berkeley National Laboratory

Lawrence Berkeley National Laboratory

Title

An electrostatic energy analyzer for longitudinal energy measurements

Permalink

https://escholarship.org/uc/item/8x7402km

Author

Sato, A.H.

Publication Date

1985-09-01

eScholarship.org Powered by the California Digital Library
University of California

HI-FAN-296

AN ELECTROSTATIC ENERGY ANALYZER FOR LONGITUDINAL ENERGY MEASUREMENTS

A. H. Sato

An electrostatic energy analyzer has been used to measure the longitudinal energy profile of the single beam transport experiment's cesium ion beam. Values for the dispersion coefficient and an estimate for the spectral resolving power are given, as well as results of the energy profile measurements on the 12mA and 0.42mA beams.

I. Introduction

Recently an electrostatic energy analyzer has been employed to measure the longitudinal energy profile of the cesium ion beams used in the single beam transport experiment (SBTE) and in the multiple beam experiment (MBE-4) now under construction. This note contains a description of the energy analyzer as well as a presentation of the results of the longitudinal energy measurements performed on SBTE.

II. Apparatus

The energy analyzer is a sector analyzer designed to present an electrostatic cylindrical field to the incoming ions. A sketch showing the analyzer's dimensions appears in Figure 1.

There are three important relations characterizing the energy analyzer. The first is the linear relation between the electrode potential difference and the kinetic energy of the ions traveling on the central path. This is:

$$T(\text{KeV}) = 0.008998 \times V(\text{volt}). \tag{1}$$

The second important relation relates the transverse displacement of the slit aperture's image produced by a group of ions to the proportional deviation of their kinetic energy from the kinetic energy of the ions on the central path. The paraxial, zero space charge derivation yields:

$$y(\text{in.}) = 18.0 \text{ in.} \times (T-T_o)/T_o \tag{2}$$

where y = transverse displacement

T = energy of the ions arriving at displacement y

T_o = energy of ions on the central path.

The constant, 18.0 in., is called the dispersion coefficient.

The final important parameter is the spectral resolving power. The central wire of the multiwire array of current collectors at the exit of the analyzer could be activated by incident ions over a range of electrode voltages even if the ions had a precisely defined energy. This effect is due to the widths of the slit aperture and detector wire, as well as aberrations, which give the image a nonzero width at the detector. This width is equivalent to an apparent energy spread in the beam, if one makes use of equation 2. The analyzer is incapable of discerning real energy spreads in the beam that are smaller than this apparent spread. A quantity of interest is the spectral resolving power, R, defined as:

$$\begin{aligned} R &= T_0/\delta T \\ &= \text{dispersion coefficient/image width} \\ \text{where } T_0 &= \text{kinetic energy of ions on the central path} \\ \delta T &= \text{apparent energy spread in the beam} \end{aligned} \qquad (3)$$

Values for R were calculated in the paraxial, zero space charge limit, and are shown in Table I.

In the paraxial, zero space charge limit, the image plane should have been 6.4 ins. above the exit of the cylindrical electrodes. However, in the experiment using the 12mA ion beam of the SBTE it was discovered that a sharper image was located at approximately 11 ins. above the electrodes. Interestingly, when the beam was attenuated to 3-1/2% of the 12mA, the best focus was achieved when the harp was located 6 to 7 ins. above the electrodes. For this reason, two values for various parameters are given in Table I. The values for the nonzero space charge case are not calculated from a derivation taking space charge into consideration. All that has been

done is to replace the drift length at the exit of the cylindrical electrodes by the observed 11 ins. instead of the calculated 6.4 ins. For this reason, these values have questionable significance.

Coarse calculations show that space charge can easily produce the displacement of the image plane by 4.6 ins. Incorporating the exact fields into the paraxial calculations is impossible since the charge density between the cylindrical electrodes is unknown. However, one can make estimates using sheets of uniform density as models for the beamlet. One then finds that the drift regions before and after the cylindrical electrodes can account for no more than 1.3 ins. of displacement. A charge density between the cylindrical electrodes not less than approximately 1/8th of the beam density of 2×10^{-5} coul/m^3 could produce the additional 3.3 ins. of displacement. The dispersion coefficient would change from 0.15% to 0.16% per wire.

A disconcerting effect of space charge is that it produces an offset in the energy vs. voltage relation that causes equation 1 to give too high an energy. For the model mentioned above, this offset is approximately 12%. Comparison with time-of-flight measurements showed no discrepancy of that magnitude. A more exact evaluation of space charge effects is required.

Not shown in Figure 1 are the widths of the cylindrical electrodes and screening electrodes. The screening electrodes are 4 ins. wide and the cylindrical electrodes are 5 ins. wide when the 1/2 in. diameter "corona rings" are included. (The "corona rings" extend the region of acceptable electric field values.[1]). In comparison, the beam width is approximately 0.8 in. at the slit aperture.

The screening electrodes control fringe field effects and make it possible to define an effective boundary to the fields, which in this device occurs approximately 0.35 in. out from the electrodes.[2] If one interprets

this as an effective increase in the path through the field region, one finds that the ideal image plane is moved 0.2 in. further away from the cylindrical electrodes' exit and the dispersion coefficient is decreased by 0.05%.

The cylindrical electrodes are held at potentials of approximately ±1/2V, where V is the total potential difference across the electrodes. The voltage dividers used to measure the electrode potentials differ slightly and cause the equipotential at the central path to be 0.32% of V below ground potential. One can estimate the acceleration of ions entering the analyzer to find that this slight offset leads to approximately 0.04% increase in the ion energies above their original values. This is below the theoretical resolving power of the analyzer.

The harp detector is similar in construction to other harps used on SBTE. The relevant changes are that the tungsten wires have a larger diameter of 20 mils and, in use, signals were taken from only one or two wires at a time.

Not shown in Figure 1 is the Tektronix 7834 oscilloscope equipped with a 7D20 plug-in unit. This was used to store signal traces from the connected harp wire and to measure the arrival time of ions at that wire.

Lastly, oscillograms of the beams' currents appear in Photographs 1 and 2, and the oscillogram of the ion accelerating voltage appears in Photograph 3. Photographs 1 and 2 provide current profiles of the beam as measured by a Deep Faraday Cup at the end of the transport channel. Two current levels were used in the procedure, one being the 12mA full beam and the other being 3-1/2% of the full beam current.

III. Procedure

A detector fixed at the end of the SBTE transport channel will be struck only by particles with the energy corresponding to the electrode potential V. If the beam pulses are all identical, then the detector will always be struck at the same time relative to the onset of a pulse. It is thus possible to use the arrival time of a group of ions at the harp to identify them as one steers them from one wire to another. This method of tracking was used in determining the dispersion coefficient.

The measurements described below were performed on the SBTE beam which exhibits a pulse-to-pulse energy jitter of approximately 0.5% over the middle of the beam pulse. The source of this jitter could not be located and remedied. The best that could be done was to use that portion of the beam which appeared to be most reproducible in its energy characteristics from one pulse to the next. The end of the pulse at the analyzer satisfied this requirement and was used in the measurements to be described. This portion of the beam pulse is not the same as the tail region of the beam as it exits the ion gun.[3] Due to space charge fields, the original beam tail is spread out as the beam travels through the transport channel. Also, some of it probably never reaches the analyzer. The beam tail at the analyzer is therefore actually composed of ions which exited the ion gun before the original beam tail ions. It is believed that the better reproducibility in arrival time of the new tail ions is due to the more rapidly changing accelerating voltage at the ion gun when that part of the beam was being created; the change in arrival time of ions of a given energy due to jitter in the accelerating voltage should be inversely proportional to the time derivative of the voltage.

Thus, to acquire data for the dispersion coefficient, the analyzer electrode potential difference was adjusted so that the wire on the central path was struck by ions from the tail of the beam pulse. The arrival time of these ions was noted as a reference. The electrode potential difference was then varied to steer the selected ions to another wire of known displacement from the central wire. The proper voltage was determined by an observed ion arrival time at the new wire that equaled the reference time. The data appear in Figure 2.

This method yields an approximate value for the dispersion coefficient. It is equivalent to changing T_o in equation 2 and neglecting the change of T_o in the denominator. However, the value of T_o changes only by 3% as the selected energy group of ions is steered over the 26 wires that were actually ever struck by ions.

The spectral resolving power was examined next. Signals from adjacent wires were examined simultaneously to see if a given energy group of ions could activate more than one wire. This method only gives a lower limit for the spectral resolving power since it incorporates into the measurement the intrinsic energy spread in the beam, as well as the response time of the detector in comparison to the time scale for energy variation seen as the beam arrives at the harp. It was desirable to use a portion of the beam where the energy changes most rapidly, and the beam tail was most suitable for this task.

The final exercise performed with the analyzer was to measure the longitudinal energy profile of the beam. The analyzer was used in a single channel mode: the electrode potential difference was selected, the arrival time of ions at the central wire was noted, and the process was repeated at a different potential. Results for the 12mA and 0.42mA beams appear in Figures 3 and 4, respectively.

IV. Results and Discussion

The data in Figure 2 indicates an energy difference of 0.15% between adjacent wires. The wire center-to-center spacing is 31 mils and this gives a dispersion coefficient of 20.7 in., which is close to the value in Table I for the full beam.

A lower limit for the spectral resolving power has been set to $T_o/\delta T \geq 333$. That is, the spread in the energy of ions striking a given wire is less than 0.3%. Note that this value is well below any of the calculated values for the 1/2m slit (see Table I) which was used in this part of the experiment. However, if one uses the sum of the slit aperture and detector wire width as the effective image width, the spectral resolving power becomes 650. Aberrations, space charge fields, and difficulty in resolving pulses separated by less than 200ns have not been considered, and are probably responsible for the factor of two degradation in the spectral resolving power.

Figures 3 and 4 present the measured longitudinal energy profile for the 12mA and 0.42mA beams. Over the flat portion of the profiles one finds two sets of points on the graphs. These reflect the lowest and highest energies measured in the beam at the noted arrival times. Due to variations between pulses one may measure energy values within the given extremes.

Most notable in the graphs are the lower energy branches at the head of the beam pulses. The acceleration of forward ions and deceleration of tail ions due to space charge forces is perceivable when comparing Figures 3 and 4. These effects have been modeled with a one-dimensional model by Faltens, Lee, and Rosenblum.[3] The ions are treated as a continuous distribution of charge, and the evolution of the beam is treated with a continuum formalism. Hence, individual ion velocities are averaged over, and phenomena (like

particles being overtaken or particles bunching at the beam head) are not always amenable to complete investigation. For this reason, measurements like those appearing in Figures 3 and 4 are of some value in understanding the condition of the beam head.

V. Acknowledgement

The author wishes to acknowledge the kind and most valuable guidance received from A. Faltens throughout the period in which this work was performed. Sincere thanks should also go to M. Tiefenback for the generous information and advice given to the author during this same period.

REFERENCES

1. A. Faltens and S. Rosenblum, Electrostatic Energy Analyzer (EEA) for HIFAR, HIFAR Note-17, (1985), unpublished.

2. Poul Dahl, Introduction to Electron and Ion Optics (New York: Academic Press, 1973), p. 48.

3. I would like to thank A. Faltens for bringing this fact to my attention.

4. A. Faltens, E.P. Lee, and S. Rosenblum, Beam Tail Erosion, unpublished.

Displacement, y, vs. Deviation in Energy, $(T-T_o)/T_o$.

Paraxial, zero space charge limit:

$$y(\text{in.}) = 18.0 \text{ in.} \times (T-T_o)/T_o$$

Paraxial case, but with image 11 in. above electrodes:

$$y(\text{in.}) = 20.6 \text{ in.} \times (T-T_o)/T_o$$

Spectral Resolving Power

If the slit width determined the maximum spectral resolving power:

	1/2mm slit	1mm slit
Paraxial, zero space charge case	1516	758
Paraxial, but with image plane 11 in. above electrodes	1734	867

If the harp wire width of 20 mils determined the maximum spectral resolving power:

Paraxial, zero space charge case	900
Paraxial, but with image plane 11 in. above electrodes	1030

TABLE I

Values for the coefficient of dispersion and spectral resolving power, as calculated in the paraxial, zero space charge limit, and also evaluated with the experimentally observed image plane position.

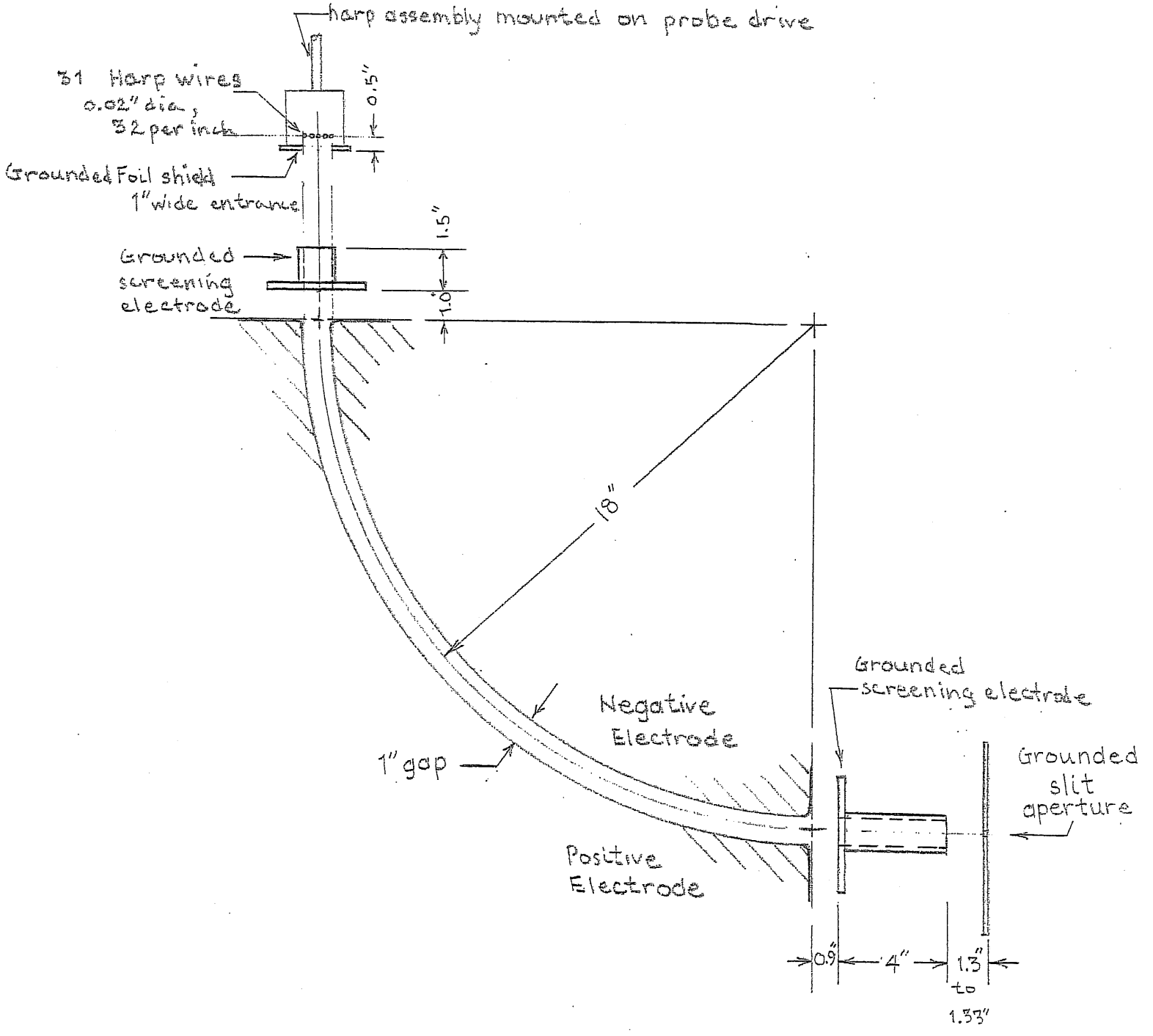

Fig 1. Energy analyzer dimensions and part locations

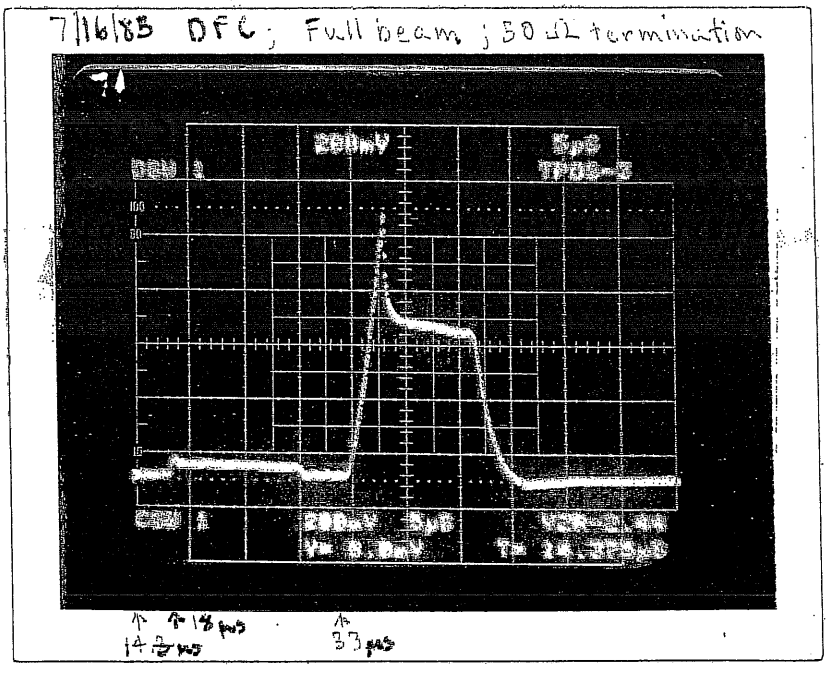

Photograph 1. Full beam current measured at the Deep Faraday Cup after quadrupole Q82. 50 ohm termination used. Horizontal scale: 5 microsecond/division. Vertical scale: 4mA/division.

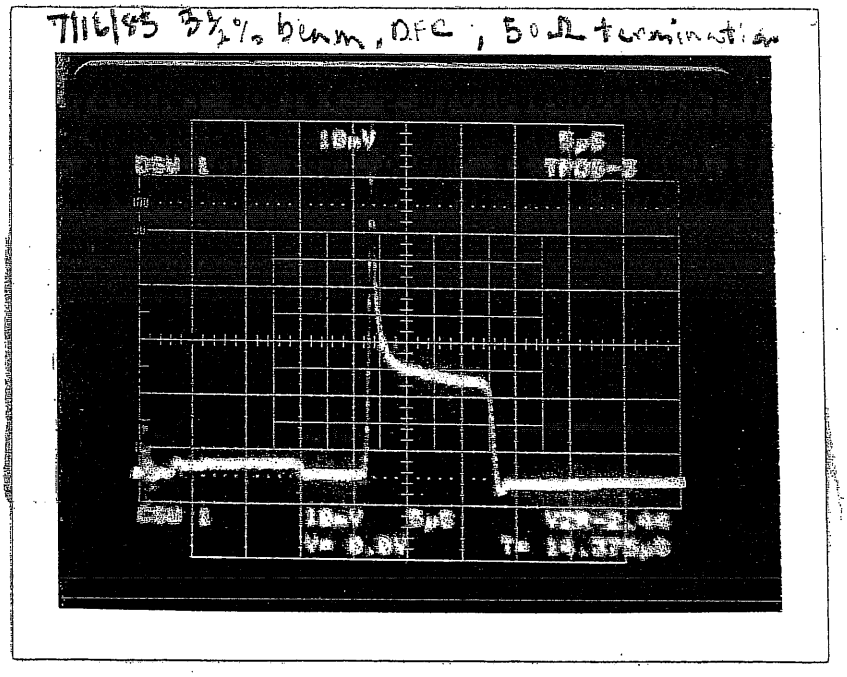

Photograph 2. Attenuated beam current, reduced to 3½% of the full beam, at the Deep Faraday Cup after Q82. 50 ohm termination used. Horizontal scale: 5 microsecond/division. Vertical scale: 0.2mA/division.

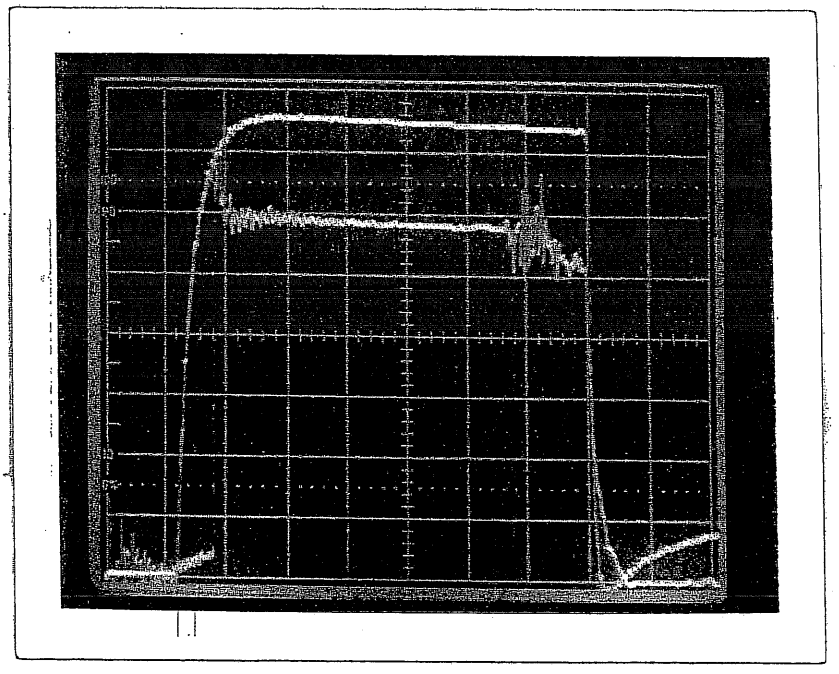

Photograph 3. High voltage pulse (top trace) at the Marx generator, and time delayed trace of the attenuated beam current measured after quadrupole Q2 with a Small Faraday Cup (lower trace). For the high voltage, the horizontal scale is 2 microsecond/division and the vertical scale is 15910 volt/division. For the current trace, the vertical scale is approximately 0.084mA/division.

Energy of wire striking wire
16 when the 122.1 kev wire are striking the noted wire

GRAPH PAPER GRAPHIC CONTROLS CORPORATION BUFFALO, NEW YORK
PRINTED IN U.S.A.
SQUARE 10 X 10 TO THE CENTIMETER AS-8014-61

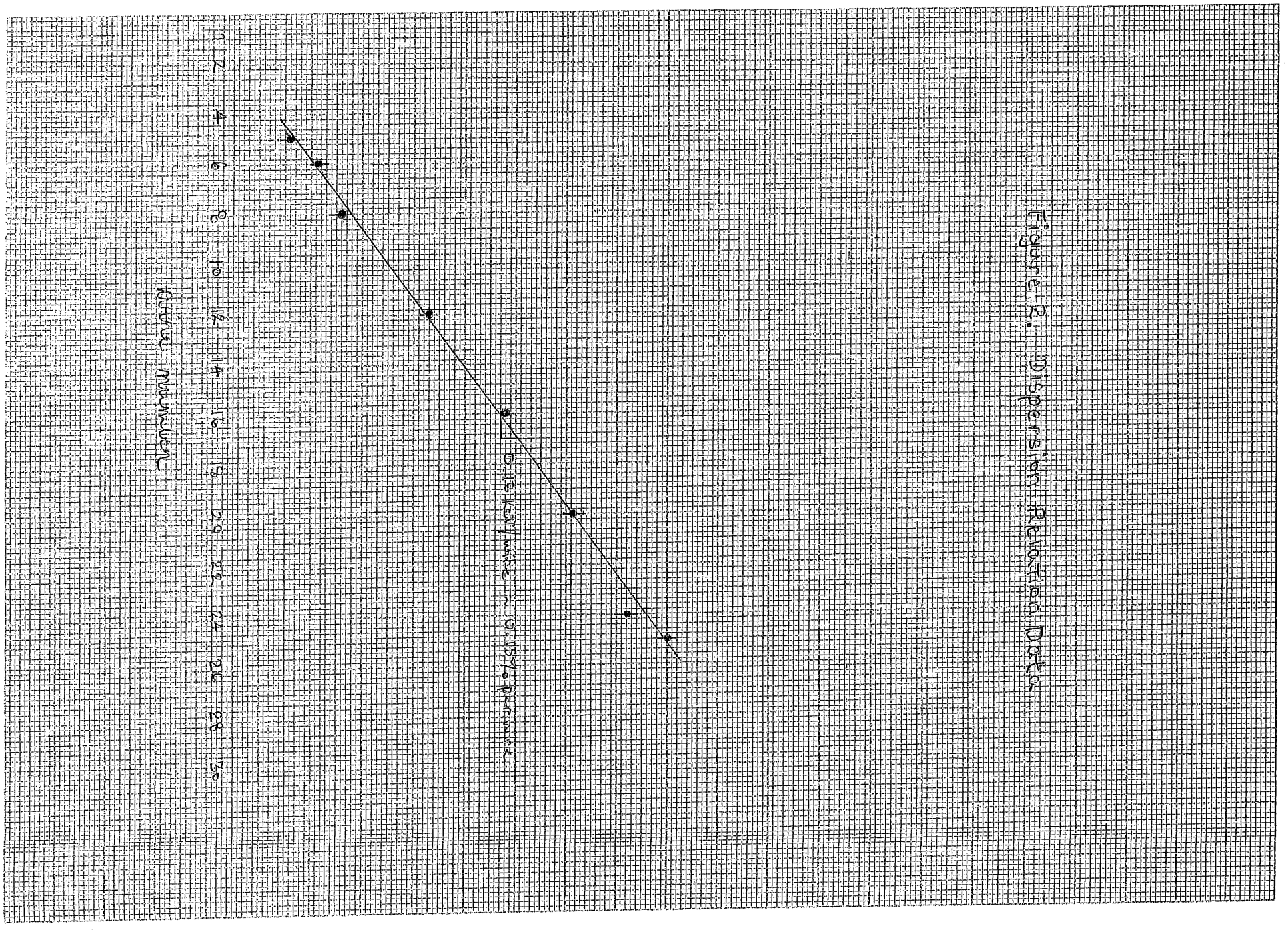

Fig. 4 Energy profile for the beam attenuated to 3±2% of the full current.

* Over the flat portion, ▭ = lower bound, ° = upper bound.

SQUARE 30 X 10 TO THE CENTIMETER AS-8014-M
GRAPHIC CONTROLS CORPORATION BUFFALO, NEW YORK
PRINTED IN U.S.A.

Fig. 3 Full beam Energy vs. Time at DFC after Q82 7/16/85 - 7/17/85